Progress in Reaction Kinetics and Mechanism, 2015, 40(3), 249–260
doi:10.3184/146867815X14262624920808 Paper: 1400302

Theoretical investigation of the mechanism and kinetics of the CH_3NH_2 +O(^{3}P) reaction

Maryam Dehestani[a]*, Razieh Naghizadeh[a] and Fahimeh Shojaie[b]

[a]*Department of Chemistry, Shahid Bahonar University of Kerman, Kerman, Iran*

[b]*International Center for Science, High Technology & Environmental Sciences, Kerman, Iran*

**E-mail: dehestani@uk.ac. ir*

ABSTRACT

We present the kinetics and mechanism of the reaction of O (^{3}P) with CH_3NH_2. Geometries of all the stationary points involved in the reaction have been investigated at the B3LYP/6-311+G (d, p) level. We report the potential energy surface for all of the possible pathways by the Gaussian-2 G3B3 method. This is the first time one has gained a conclusive insight into the detailed mechanism and kinetics for this reaction. Using the Rice–Ramsperger–Kassel–Marcus (RRKM) theory, we have computed the rate constants for channels leading to several products over the temperature range 298–440 K. The main reaction channel is found to be addition of an oxygen atom to CH_3NH_2 followed by migration of an H atom from N to O atoms and loss of H_2O, which agrees with experimental results (Slagle, Dudich, and Gutman (1979) *J. Phys. Chem*., 83). As experimental data are available for this reaction, we are able to conclude that our thermal rate constants are in agreement over a wide range of temperatures.

KEYWORDS: multichannel-RRKM theory, G3B3 method, *ab initio* calculations, CH_3NH_2, O(^{3}P)

1. INTRODUCTION

Methylamine (CH_3NH_2) is not only the simplest primary amine but also a very important molecule in organic syntheses, and biological, and atmospheric processes [1]. CH_3NH_2 is produced in Jupiter's upper troposphere and lower stratosphere, by recombination of NH_2 with methyl radicals, which are formed by reaction of hot hydrogen atoms with methane. Photolysis of ammonia, phosphine, and acetylene produce these hot hydrogen atoms [2].

Methylamines are highly alkaline substances, and slightly toxic, which can irritate the digestive tract. The decomposition of methylamine gives methyleneimine which is highly toxic [3]. Since there is much atomic oxygen in the atmosphere, which is produced by the decomposition of ozone, the reaction of O(^{3}P) with CH_3NH_2 might be one of the most efficient and important ways to eliminate CH_3NH_2.

This reaction can proceed via the following possible reaction pathways: (a) H atom abstraction from the C–H bonds; (b) H atom abstraction from the N–H bonds; and (c) addition of oxygen atom to CH_3NH_2 [4].

It is seen that the rate constants increase along the series CH_3NH_2, $C_2H_5NH_2$, $(CH_3)_2NH$, and $(CH_3)_3N$ at room temperature, which shows that H atom abstraction from N–H bonds is not the predominant reaction pathway, but it is rather consistent with either H atom abstraction from the C–H bonds or with formation of an addition product [4].

One possible pathway for this reaction can be related to attachment of the oxygen atom to methylamine and rearrangement as follows [4]:

$$CH_3NH_2 + O\ (^3P) \rightarrow CH_3NHOH \qquad (1)$$

Slagle *et al*. [5] studied reactions of O atom with six amines; mono-, di-, and tri-methylamine and –ethylamine at ambient temperature in a cross-jet reactor. They revealed details of the mechanism of reactions of O atom with the amines, *i.e*. that for primary and secondary amines, in the first step, O atom adds to form an energy-rich amine N-oxide. The second pathway with high probability is migration of H atom to O atom from the N atom. The last step is decomposition of the excited hydroxylamine in three ways, OH loss, H_2O loss or R loss. The first way (OH loss) is usually dominant [5].

Here, we are primarily interested in understanding the mechanisms and products involved in the title reaction in details and the dependence of the rate constants and branching ratio on the temperature. Here we report detailed *ab initio* calculations to study the mechanisms of the title reaction almost completely for the first time. We present the RRKM calculation to check the kinetics of the multichannel reaction.

2. COMPUTATIONAL METHODS

Theoretical calculations were carried out for the title reaction using the Gaussian 03 program [6]. The B3LYP/6-311+G (d, p) level of theory was used to study the geometry of all of the species involved in this investigation. To verify the nature of reactants (R), transition states (TS), intermediates (IM), and products (P), and providing the zero point energy (ZPE) corrections, harmonic vibrational frequencies were calculated at the same level. Then, intrinsic reaction coordinate (IRC) [7–9] calculations were used to confirm the transition state (TS) geometries. The single-point energies were calculated using the G3B3 method at the B3LYP/6-311+G (d, p) optimised geometries to obtain more reliable energies of all the stationary points on the potential energy surface (PES). The RRKM method has been employed to calculate the total and individual rate constants and the branching ratio for the various product channels.

3. RESULTS AND DISCUSSION

The optimised structures of all reactants, products, intermediates and transition states involved in the reaction of $CH3NH_2$ with O (^3P) in this investigation are depicted in Figure 1 along with experimental geometries [10]. The potential energy profile for the title reaction calculated at the G3B3 method is shown in Figure 2. The ZPE corrections and relative energies (relative to the reactants of CH_3NH_2 + O) at the levels of the B3LYP and the G3B3 are listed in Table 1. We have used the G3B3 method to obtain more reliable energies for rate constant calculation. Table 2 exhibits the moments of inertia and vibrational frequencies for the various species involved in the $CH3NH_2$ + O (^3P) reaction at the B3LYP/6-311+G (d, p) level of theory.

Mechanisms

The reaction of CH_3NH_2 with O (^3P) forms the intermediate IM1 through the transition state TS1. All the vibrational frequencies of IM1 are positive, which indicate the molecular complex IM1 is a stable structure, the barrier of TS1 is 7.20 kcal mol^{-1}. From IM1, four rearrangement situations are possible to form different products:

(1) CH_3NHOH, and CH_3N+H_2O formation. The IM1 forms product CH_3NHOH (P1) via transition state TS2. In IM1 the N–H bond is broken and in TS2 the O–H bond is shortened by 0.74 Å. The barrier of TS2 is 16.05 kcal mol^{-1} below the reactants. P1 forms product CH_3N+H_2O via transition state TS3. In P1 the N–H bond is broken and in TS3 the N–O bond is lengthened by 0.51 Å. TS3 lies 2.53 kcal mol^{-1} higher in energy than the reactants.

Table 1 Relative energies and ZPE corrections of reactants, intermediates, transition states and products involved in the CH_3NH_2 + O (^3P) reaction, in kcal mol^{-1}

Species	ZPE	B3LYP/6-311+G(d,p)	G3B3
R(CH_3NH_2)	40.35	0.00	0.00
IM1	43.54	–42.07	–45.15
IM2	43.09	–92.62	–101.76
TS1	41.04	5.85	7.20
TS2	40.07	–13.10	–16.05
TS3	36.84	–2.91	–2.53
TS4	39.80	–4.45	–7.42
TS5	37.03	9.98	5.01
TS6	39.52	52.86	57.04
TS7	36.85	–19.71	–19.97
TS8	36.81	–24.36	–21.78
P1(CH_3NHOH)	42.91	–62.20	–66.07
P2(CH_3N+H_2O)	38.65	–8.07	–7.28
P3(CH_2NH_2+OH)	42.43	–24.83	–26.98
P4(CH_3NO+H_2)	33.47	–12.61	–20.00
P5(NH_2CHO+H_2)	36.11	–88.08	–92.40
P6(CH_2O+NH_3)	41.56	–80.51	–81.61

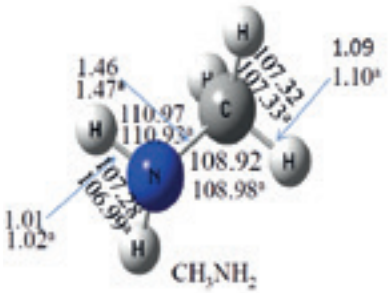
H
1.09
1.10
1.46
1.47
110.97
110.93
C
H
N
108.92
108.98
H
1.01
1.02
H
CH3NH2

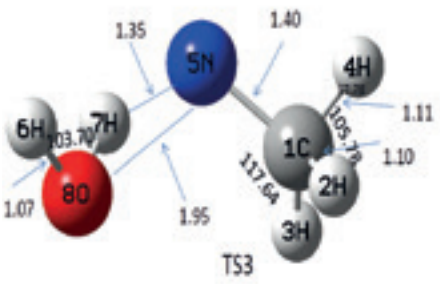
1.35
1.40
5N
4H
1.11
6H
7H
1C
1.10
2H
1.07
8O
1.95
3H
TS3

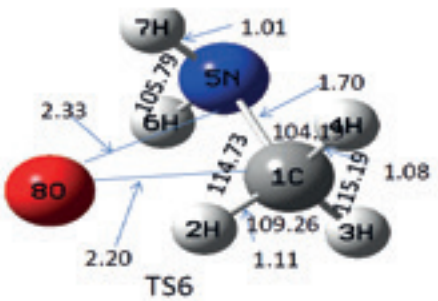
7H
1.01
5N
1.70
2.33
6H
4H
8O
1.08
1C
2H
3H
2.20
1.11
TS6

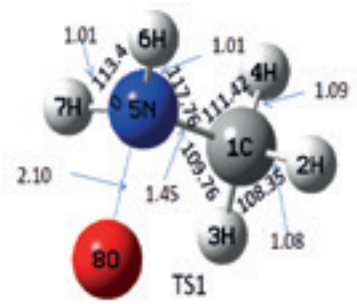
1.01
6H
1.01
7H
5N
4H
1.09
1C
2H
2.10
1.45
3H
1.08
8O
TS1

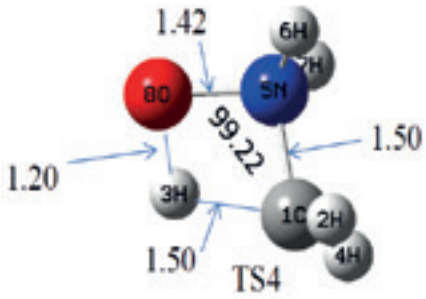
1.42
6H
8O
5N
7H
1.50
1.20
3H
1C
2H
4H
1.50
TS4

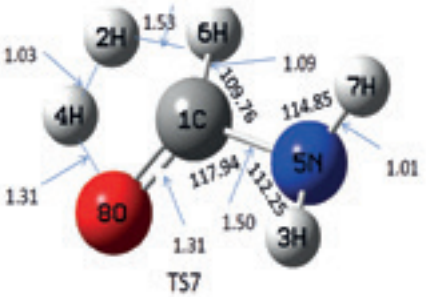
2H
1.53
6H
1.03
1.09
4H
1C
7H
1.31
5N
1.01
8O
1.50
3H
1.31
TS7

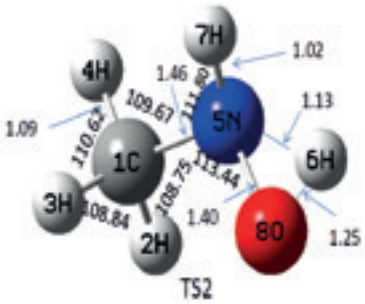
7H
1.02
4H
1.13
1.09
5N
1C
6H
3H
1.40
8O
1.25
2H
TS2

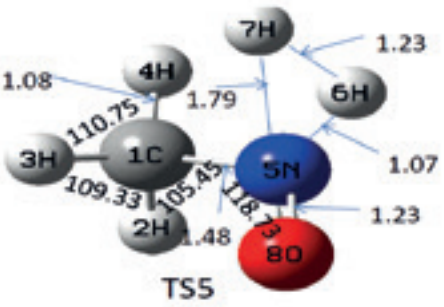
7H
1.23
1.08
4H
1.79
6H
3H
1C
5N
1.07
2H
1.23
1.48
8O
TS5

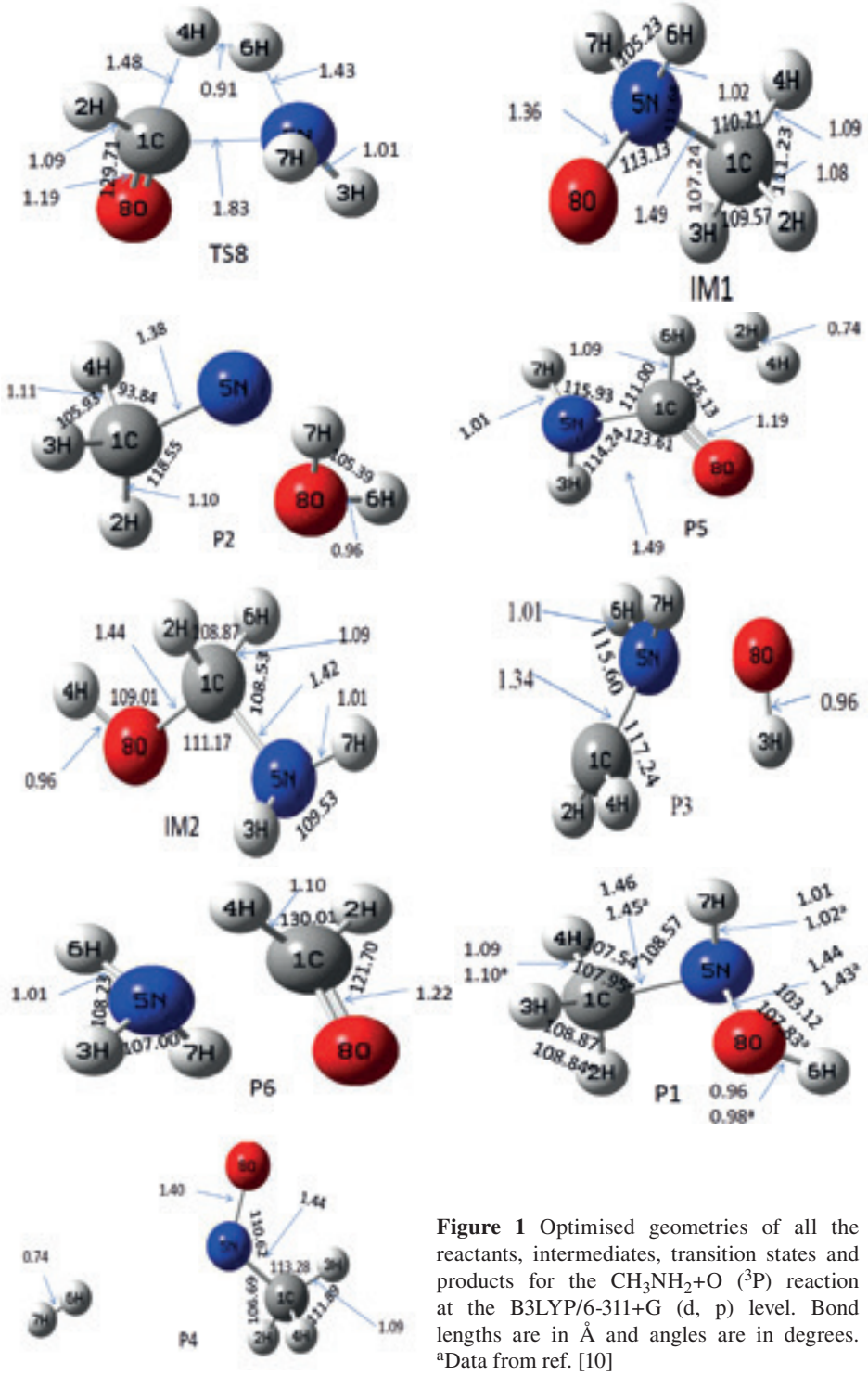

Figure 1 Optimised geometries of all the reactants, intermediates, transition states and products for the CH_3NH_2+O (^{3}P) reaction at the B3LYP/6-311+G (d, p) level. Bond lengths are in Å and angles are in degrees. [a]Data from ref. [10]

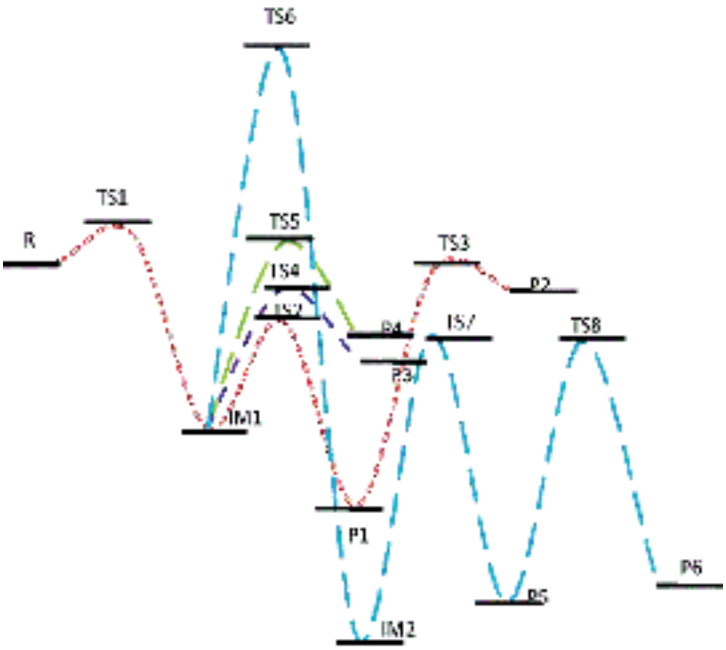

Figure 2 Schematic energy profile of the potential energy surface for the CH_3NH_2+O (^3P) reaction system at the G3B3 level.

(2) CH_2NH_2+OH formation. IM1 forms product CH_2NH_2+OH via transition state TS4. In TS4 the N–O bond is lengthened by 0.06 Å. The barrier at TS4 is 7.42 kcal mol^{-1} below the reactants.
(3) CH_3NO+H_2 formation. IM1 forms product CH_3NO+H_2 via transition state TS5. In IM1, the two N–H bonds are broken and in TS5 the N–O bond is shortened by 0.13 Å. TS5 lies 5 kcal mol^{-1} above the reactants.
(4) NH_2CHO+H_2, and CH_2O+NH_3 formation. IM1 forms IM2 via transition state TS6. In IM1 the N–O bond is broken, and in TS6 the C–H bond is lengthened by 0.03 Å. The barrier of TS6 is 57.04 kcal mol^{-1} higher than that of the reactants. IM2 forms product NH_2CHO+H_2 (P5) through the transition state TS7. In IM2 the O–H bond is broken and in TS7 the C–H bond is lengthened by 0.44 Å. The barrier of TS7 is 19.97 kcal mol^{-1} below the reactants. P5 forms product CH_2O+NH_3 through transition state TS8. In P5 the C–N bond is broken and in TS8 the C–H and N–H bonds are shortened and begin to form. The barrier of TS8 is 21.78 kcal mol^{-1} below the reactants.
As to the mechanisms stated above, the dominant channel of the title reaction is addition of oxygen atom to CH_3NH_2. Although the other channels cannot take place at room temperature, because they have high barriers, we calculated the rate constants for all of the channels in forming different products to study the dependence of the rate constants and branching ratio on temperature.

Table 2 Vibrational frequencies (cm^{-1}) and moments of inertia (amu) for various species for the CH_3NH_2 + O (^3P) reaction at the B3LYP/6-311+G (d, p) level of theory

Species	I_a, I_b, I_c	Frequencies
CH_3NH_2	17.4,79.7,83.0	309,824,974,1047,1163,1342,1457,1497,1516,1666,2963,3056, 3092,3506,3585
CH_2NH_2	12.2,65.8,76.1	434,583,631,932,1219,1315,1474,1653,3142,3255,3557,3659
NH_2CHO	26.1,171.2,196.4	375,525,579,854,1011,1136,1379,1583,1731,2999,3555,3692
NH_3	5.9,5.9,9.8	924,1659,1659,3492,3629,3629
CH_2O	6.3,46.2,52.6	1199,1260,1530,1813,2878,2936
CH_3N	11.6,75.6,75.6	960,960,1044,1379,1419,1419,2935,2995,2995
H_2O	2.1,4.2,6.3	1591,3843,3952
OH	0.0,3.2,3.2	3721
CH_3NH	14.1,70.9,74.3	261,953,1006,1050,1330,1394,1475,1485,2931,2970,3090,3382
H_2	0.0,0.09,0.09	4402
CH_3NO	29.1,157.8,175.7	165,576,840,970,1153,1371,1448,1452,1663,3017,3098,3129
CH_3NH_2O	46.8,178.3,204.1	279,436,873,889,974,1175,1195,1384,1431,1440,1464,1500, 1649,3027,3132,3164,3225,3235
IM1	46.5,178.5,204.0	272,435,876,889,979,1176,1198,1351,1430,1445,1464,1500, 1650,3031,3137,3169,3221,3229
IM2	44.1,185.8,211.4	181,249,505,707,953,1017,1102,1237,1255,1349,1465,1531,1655, 2918,3005,3538,3633,3836
TS1	60.3,261.8,300.7	284i,191,239,513,725,934,1062,1144,1298,1453,1485,1492, 1642,3008,3116,3155,3571,3676
TS2	43.5,181.4,204.6	1848i,232,381,760,932,1115,1162,1198,1209,1436,1441,1472, 1503,2789,3021,3095,3131,3406
TS3	49.2,241.1,272.6	841i,235,312,451,836,885,1115,1153,1187,1342,1356,1521,1565, 2314,2629,2908,2966,2996
TS4	55.8,156.7,191.0	1564i,235,757,823,861,921,1057,1168,1183,1269,1284,1468, 1657,2061,3064,3147,3412,3472
TS5	50.1,173.4,201.8	1272i,269,506,605,706,913,1033,1166,1252,1403,1444,1453, 1491,1527,2792,3052,3131,3158
TS6	102.2,180.2,260.9	1227i,196,283,328,502,791,897,1000,1190,1306,1381,1423, 1615,2595,3106,3207,3498,3590
TS7	45.9,192.1,214.6	2355i,316,425,559,644,687,857,1057,1153,1236,1351,1440, 1590,1738,1962,3036,3532,3657
TS8	47.0,224.5,244.4	1561i,273,311,493,646,771,870,967,1187,1264,1341,1395,1571, 1783,2309,3051,3478,3595

The changes of the bond length along the minimum energy path (MEP) for the P1 channel via TS2 as a function of the intrinsic reaction coordinate (s) are described in Figure 3. As shown in Figure 3, the active O–H and N–H bonds change strongly in the course of this reaction, while the other bond lengths are almost invariant during the reaction process. The breaking N–H bond elongates linearly with s after about s = –0.5 $(amu)^{1/2}$ bohr, and the forming O–H bond shortens rapidly and arrives at the bond length of O–H in H_2O molecule at about s = 1.0$(amu)^{1/2}$ bohr. Thus, it is evident that the geometric changes mainly take place in the region

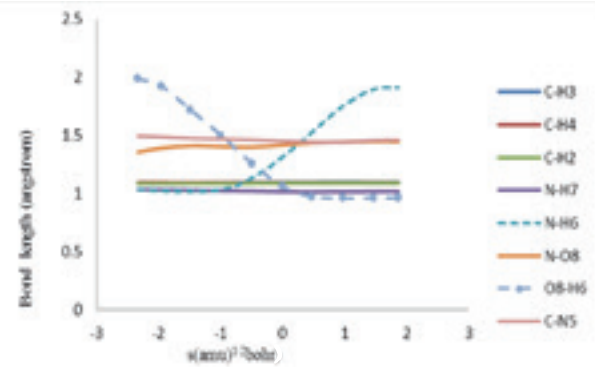

Figure 3 The changing of some key bond distances along the reaction coordinate for IM1 channel at the B3LYP/6-311+G (d, p) level.

of s from –0.5 to 1.0 $(amu)^{1/2}$ bohr. Similar conclusions also obtain for the other channels.

Rate constant calculation

The reaction scheme employed in the calculation is as follows:

$$CH_3NH_2 + O(R) \underset{k_1}{\overset{a}{\rightleftarrows}} IM1^* \xrightarrow{k_2} CH_3NHOH \quad (P1)$$

$$CH_3NH_2 + O(R) \underset{k_1}{\overset{a}{\rightleftarrows}} IM1^* \xrightarrow{k_2} P1 \xrightarrow{k_7} CH_3N + H_2O \quad (P2)$$

$$CH_3NH_2 + O(R) \underset{k_1}{\overset{a}{\rightleftarrows}} IM1^* \xrightarrow{k_3} CH_2NH_2 + OH \quad (P3)$$

$$CH_3NH_2 + O(R) \underset{k_1}{\overset{a}{\rightleftarrows}} IM1^* \xrightarrow{k_4} CH_3NO + H_2 \quad (P4)$$

$$CH_3NH_2 + O(R) \underset{k_1}{\overset{a}{\rightleftarrows}} IM1^* \underset{k_6}{\overset{k_5}{\rightleftarrows}} IM2^* \xrightarrow{k_8} NH_2CHO + H_2 (P5)$$

$$CH_3NH_2 + O(R) \underset{k_1}{\overset{a}{\rightleftarrows}} IM1^* \underset{k6}{\overset{k5}{\rightleftarrows}} IM2^* \xrightarrow{k_8} P5 \xrightarrow{k_9} NH_3 + CH_2O \quad (P6)$$

$$IMj^* \xrightarrow{\omega_i} IMj$$

The steady-state approximation for all the excited intermediates leads to the following expressions for the second-order rate constants of the various product channels:

$$k_{P1}(T,P) = \frac{\alpha_a}{h} \frac{Q_t^+ Q_r^+}{Q_{CH_3NH_2} Q_O} e^{-E_a/RT} \int_0^\infty \frac{X_2 k_2}{Y} N_0(E^+) \exp\left(-\frac{E^+}{RT}\right) dE^+$$

$$k_{P2}(T,P) = \frac{\alpha_a}{h}\frac{Q_t^+ Q_r^+}{Q_{CH_3NH_2} Q_O} e^{-E_a/RT} \int_0^\infty \frac{k_2 k_7 X_2}{Y} N_0(E^+) \exp\left(-\frac{E^+}{RT}\right) dE^+$$

$$k_{P3}(T,P) = \frac{\alpha_a}{h}\frac{Q_t^+ Q_r^+}{Q_{CH_3NH_2} Q_O} e^{-E_a/RT} \int_0^\infty \frac{X_2 k_3}{Y} N_0(E^+) \exp\left(-\frac{E^+}{RT}\right) dE^+$$

$$k_{P4}(T,P) = \frac{\alpha_a}{h}\frac{Q_t^+ Q_r^+}{Q_{CH_3NH_2} Q_O} e^{-E_a/RT} \int_0^\infty \frac{X_2 k_4}{Y} N_0(E^+) \exp\left(-\frac{E^+}{RT}\right) dE^+$$

$$k_{P5}(T,P) = \frac{\alpha_a}{h}\frac{Q_t^+ Q_r^+}{Q_{CH_3NH_2} Q_O} e^{-E_a/RT} \int_0^\infty \frac{k_5 k_8}{Y} N_0(E^+) \exp\left(-\frac{E^+}{RT}\right) dE^+$$

$$k_{P6}(T,P) = \frac{\alpha_a}{h}\frac{Q_t^+ Q_r^+}{Q_{CH_3NH_2} Q_O} e^{-E_a/RT} \int_0^\infty \frac{k_5 k_8 k_9}{Y} N_0(E^+) \exp\left(-\frac{E^+}{RT}\right) dE^+$$

$$k_{IM1}(T,P) = \frac{\alpha_a}{h}\frac{Q_t^+ Q_r^+}{Q_{CH_3NH_2} Q_O} e^{-E_a/RT} \int_0^\infty \frac{\omega X_2}{Y} N_0(E^+) \exp\left(-\frac{E^+}{RT}\right) dE^+$$

$$k_{IM2}(T,P) = \frac{\alpha_a}{h}\frac{Q_t^+ Q_r^+}{Q_{CH_3NH_2} Q_O} e^{-E_a/RT} \int_0^\infty \frac{\omega k_5}{Y} N_0(E^+) \exp\left(-\frac{E^+}{RT}\right) dE^+$$

with the following definitions:

$$X_1 = k_1 + k_2 + k_3 + k_4 + k_5 + \omega$$

$$Y = X_1 X_2 - k_5 k_6 X_2 = k_6 + k_8 + \omega$$

where α_a is the statistical factor (degeneracy) for the association step. Q_t^+ and Q_r^+ are the translational and rotational partition functions of the variational "transition state" for the association, respectively. $Q_{CH_3NH_2}$ and Q_0 are the total partition functions of CH_3NH_2 and O, respectively. E_a is the barrier for the association. $N_0(E^+)$ is the number of states for the association "transition state". The overall rate constant corresponds to the sum of the above eight rate constants. The branching ratios for each product channel are calculated as the ratio of the individual rate constants to the overall rate constant.

By using RRKM theory, the microcanonical rate constant can be written as:

$$k_i(E) = \kappa_i C_i \frac{N(E-E_i^*)}{h\,\rho_j(E)},\ i=1,2,\ldots,8;\ j=1,2$$

where C_i is the ratio of the overall rotational partition function of the TSi (i=1, 2,…, 8) and the intermediate IMj (1, 2,); h is Planck's constant; $\rho_j(E)$ is the density of states at energy E of the intermediate j; $N(E–E_i^*)$ is the number of states at the

energy above the barrier height E_i^* for transition state i and κ_i is the tunnelling factor. It is convenient to evaluate this factor using the Eckart potential [11]. A rotor approximation [12-15] has been used in the multichannel RRKM calculations since several structures have small vibrational frequencies below 100 cm^{-1} (see Table 2). The calculations of density of states and the number of states were performed using the Beyer–Swinehart algorithm [16, 17]. The collision deactivation rate (ω) is written as $ß_c Z_{LJ}$[He], where $ß_c$ is the collision efficiency and is obtained using Troe's weak collision approximation [18] with the energy transfer parameter–<ΔE> (the average energy transferred per collision). Z_{LJ} and [He] are the Lennard-Jones collision frequency and the concentration of the helium bath gas, respectively. Here we use the weak collision approximation for each intermediate and assume that the collisional rates are same for all intermediates for simplicity [19]. –<ΔE> is unknown and cannot be calculated quantitatively. In consideration of the experimental rate constants measured at different pressures, these were estimated by Lim and Gilbert's biased random walk (BRW) model (200–1000 K) –<ΔE> / cm^{-1}=0.6T-41 for helium atom [20]. To estimate the collision efficiency we have used the Lennard–Jones potential by fitting the interaction energies calculated at the G3B3/6-311+G (d, p) level for IM1...He (the corresponding Lennard–Jones potential parameters are given in the caption to Figure 4).

The RRKM-calculated total and individual rate constants over the temperature range of 298–440 K at a pressure of 26 torr are shown in Table 3 along with the comparison with experimentally known values [4]. Figure 5 shows the logarithm of calculated rate constants *versus* temperature. As can be seen in Figure 5, the total

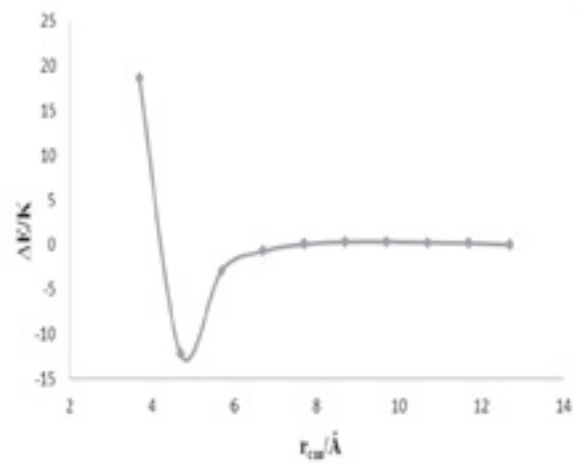

Figure 4 The B3LYP/6-311+G (d, p) calculated intermolecular interaction energy between IM1 and the helium bath gas. r_{cm} represents the separation of the centre of mass of the IM1 and He atom. The Lennard–Jones potential well (σ=12.22 K) and the collisional diameter (ε=4.54 Å) are estimated.

Table 3 Calculated rate constants ($cm^3molecule^{-1}s^{-1}$) for the CH_3NH_2 + O (^{3}P) reaction in the temperature range 298–440 K

k_{exp}[a]	k_t	k_{P6}	k_{P5}	k_{P4}	k_{P3}	k_{P2}	k_{P1}	k_{IM2}	k_{IM1}	T(K)
5.65E-13	3.72E-13	2.44E-16	1.29E-20	2.11E-16	2.72E-16	6.83E-16	2.55E-23	4.19E-16	3.7E-13	298.0
7.58E-13	6.67E-13	3.11E-16	1.68E-20	3.41E-16	3.88E-16	1.16E-15	4.3E-23	6.59E-16	6.64E-13	336.6
1.01E-12	3.37E-12	1.09E-15	6.1E-20	1.61E-15	1.8E-15	5.26E-15	1.88E-22	3.02E-15	3.35E-12	385.6
1.4E-12	1.58E-12	4.07E-16	2.4E-20	7.31E-16	7.96E-16	2.29E-15	7.75E-23	1.36E-15	1.57E-12	439.0
	1.62E-12	4.13E-16	2.44E-20	7.46E-16	8.12E-16	2.33E-15	7.91E-23	1.39E-15	1.61E-12	440.0

[a]Data from ref.[4].

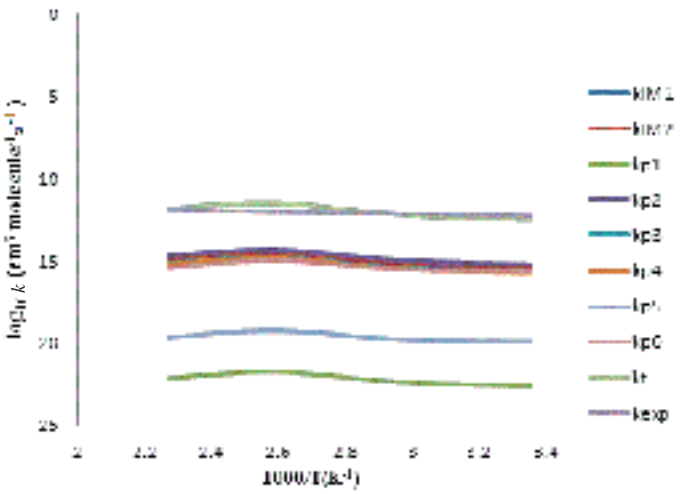

Figure 5 Logarithm of calculated rate constants as a function of 1000/ *T* for the CH_3NH_2+O (^{3}P) reaction.

rate constants vary with temperature. Over the temperature range of 298–440 K, the total rate constants are fitted to a three-parameter expression which can be obtained as follows:

$$k=8.76\times10^{-12}\ T^{0.02}\ e^{-1648/R\ T}\ (cm^3\ molecule^{-1}\ s^{-1})$$

where R is the general gas constant and equal to 1.987 cal mol^{-1} K^{-1}.
Atkinson *et al.* [4] reported the following expression for the measured rate constant for this reaction between 298 and 440 K using experimental data [4]:

$$k=9.02\times10^{-12}e^{-1650/RT}\ (cm^3\ molecule^{-1}\ s^{-1})$$

As listed in Table 3, the main channel is formation of the primary amine N-oxide (IM1) and its rearrangement to hydroxylamine by H-atom migration from N to O (formation of P1) and finally formation of P2 by decomposition of P1, and other channels such as IM2, P1, P3, P4, P5 and P6 are negligible. The first (formation of IM1) and second (formation of P1) steps are in agreement with the experimental work of Slagle *et al.* [5]. They showed that the final step is decomposition of hydroxylamine to CH_3NH+OH and other possible products of this reaction are

CH_2NH+H_2O and CH_3HNO+H. Our study indicates the dominant product is CH_3N+H_2O (P2).

4. CONCLUSIONS

In this paper, the mechanism and kinetics of the reaction between CH_3NH_2 and O (^3P) were investigated employing *ab initio* methods along with RRKM theory. The results show that the dominant channel is the addition of the oxygen atom to CH_3NH_2 to form IM1 (an energy-rich amine N-oxide), and then migration of H-atom to the O atom from the N atom (formation of P1), and the final step is decomposition P1. The results are in good agreement with the available experimental values over the temperature range 298–440 K. Over this temperature range the overall rate constant obtained in the present study (k=8.76×10^{-12} T$^{0.02}$ e$^{-1648/RT}$ cm^3 molecule^{-1} s^{-1}) is in agreement with the expression reported by Atkinson and Pitts (k=9.02×10^{-12}e$^{-1650/RT}$ cm^3 molecule^{-1} s^{-1}) [4].

REFERENCES

[1] Tian, W., Wang, W., Zhang, Y. and Wang, W. (2009) *Int. J. Quantum Chem*., **109**, 1566-1575.
[2] Kaye, J.A. and Strobel, D.F. (1983) Icarus, **55**, 399-419.
[3] Pan, Y., Tang, Y. and Wang, R. (2011) *Comp. Theor. Chem*., **965**, 298-304.
[4] Atkinson, R. and Pitts Jr., J.N. (1978) *J. Chem. Phys*., **68**, 911-915.
[5] Slagle, I.R., Dudich, J.F. and Gutman D. (1979) *J. Phys. Chem*. **83**, 3065-3070.
[6] Frisch, M.J., Trucks, G.W., Schlegel, H.B., Scuseria, G.E., Robb, M.A., Cheeseman, J.R., *et al. Gaussian 03* (Revision B.03), Gaussian, Inc., Pittsburgh PA.
[7] Gonzalez, C. and Schlegel, H.B. (1989) *J. Chem. Phys*., **90**, 2154-2161.
[8] Gonzalez, C. and Schlegel, H.B. (1990) *J. Phys. Chem*., **94**, 5523-5527.
[9] Fukui, K. (1981) *Act. Chem. Res*., **14**, 363-368.
[10] Chattaraj, P.K., Sarkar, U., Parthasarathi, R. and Subramanian, V. (2005) *Int. J. Quantum Chem*., **101**, 690-702.
[11] Johnston, H.S. and Heicklen, J. (1962) *J. Phys. Chem*., **66**, 532-533.
[12] Ayala, P.Y. and Schlegel, H.B. (1998) *J. Chem. Phys*., **108**, 2314-2325.
[13] Truhlar, D.G. (1991) *J. Comput. Chem*., **12**, 266-270.
[14] Pitzer, K.S. (1953) *Quantum chemistry*. Prentice-Hall, Englewood Cliffs.
[15] Pitzer, K.S. and Gwinn, W.D. (1942) *J. Chem. Phys*., **10**, 428-439.
[16] Stein, S. E. and Rabinovitch, B. S. (1973) *J. Chem. Phys*., **58**, 2438-2445.
[17] Astholz, D. C., Troe, J. and Wieters, W. (1979) *J. Chem. Phys*., **70**, 5107-5116.
[18] Troe, J. (1977) *J. Chem. Phys*., **66**, 4745-4757.
[19] Marchand, N., Rayez, J. C. and Smith, S. C. (1998) *J. Phys. Chem., A* **102**, 3358-3367.
[20] Lim, K. F. and Gilbert, R. G. (1990) *J. Chem. Phys*., **92**, 1819-1830.